https://doi.org/10.5194/egusphere-2025-2034
Preprint. Discussion started: 27 May 2025
© Author(s) 2025. CC BY 4.0 License.

Distribution and fluxes of marine particles in the South China Sea continental slope: implications for carbon export

Shujin Guo[1, 2†], Mingliang Zhu[1, 2†], Wenlong Xu[3], Shan Zheng[1, 2], Sumei Liu[4], Ying Wu[5], Juan Du[1, 2], Chenhao Zhao[1], Xiaoxia Sun[1, 2, 6]

[1]Jiaozhou Bay National Marine Ecosystem Research Station, Institute of Oceanology, Chinese Academy of Sciences, Qingdao 266071, China

[2]Laboratory for Marine Ecology and Environmental Science, Qingdao Marine Science and Technology Center, Qingdao 266237, China

[3]Ocean College, Jiangsu University of Science and Technology, Zhenjiang 212100, China

[4]Frontiers Science Center for Deep Ocean Multispheres and Earth System, and Key Laboratory of Marine Chemistry Theory and Technology, Ministry of Education, Ocean University of China, Qingdao 266100, China

[5]State Key Laboratory of Estuarine and Coastal Research, Faculty of Earth Sciences, East China Normal University, Shanghai 201100, China

[6]University of Chinese Academy of Sciences, Beijing 100049, China

Correspondence to: Xiaoxia Sun (xsun@qdio.ac.cn)

Abstract. Marine particles are key vectors in the ocean's biological carbon pump, yet their distribution, contributions to particulate organic carbon (POC) flux, and the mechanisms controlling these processes remain poorly understood in marginal seas. In this study, we investigated the spatial distribution and carbon export potential of marine particles along the continental slope of the South China Sea (SCS), using *in situ* imaging data from an Underwater Vision Profiler (UVP 5) collected during a June 2015 cruise. Particle abundances ranged from 0 to 783 particles L^{-1} (mean: 68 ± 69 particles L^{-1}), with small particles (ESD < 500 μm) dominating in number (>97%) but contributing less to POC flux (mean = 23.8% ± 11.5%) than large particles (76.2% ± 11.5%). Particle abundance and volume concentration were significantly higher in waters shallower than 200 m than in deeper waters ($p < 0.01$), reflecting elevated surface particles production. Estimated POC fluxes ranged from 3.4 to 302.4 mg C m^{-2} d^{-1}, with maxima in the upper 100 m and at stations influenced by cyclonic eddies. In contrast, anticyclonic eddies were associated with reduced particle concentrations and export, likely due to stratification and nutrient limitation. The relative contribution of small particles to total POC flux increased with depth, suggesting progressive disaggregation of large particles in the mesopelagic zone. These results reveal strong spatial and vertical variability in particle-mediated carbon export and underscore the role of mesoscale physical processes in regulating carbon flux along the SCS slope.

Key words: marine particles, Underwater Vision Profiler, particulate organic carbon (POC) flux, particle size distribution, mesoscale eddies, South China Sea, continental slope, biological pump

† These authors contributed equally to this work.

https://doi.org/10.5194/egusphere-2025-2034
Preprint. Discussion started: 27 May 2025
© Author(s) 2025. CC BY 4.0 License.

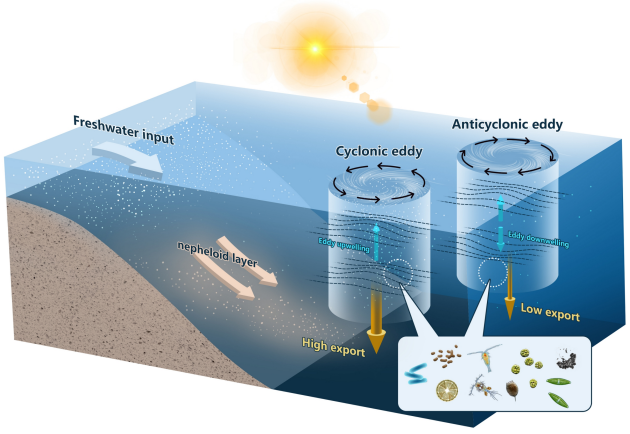

1 Introduction

Marine particles are critical components of the oceanic carbon cycle, serving as vehicles for transporting organic carbon from the surface ocean to the deep sea via the biological pump (Siegel et al., 2022). These particles, which include a diverse array of forms such as micron-scale phytoplankton cells, submillimeter detrital fragments, millimeter-scale aggregates, and zooplankton fecal pellet, play an essential role in global carbon dynamics (Turner, 2015). The transport of marine particles from surface waters to deeper layers is a primary mechanism for sequestering carbon in the deep ocean, effectively isolating it from the atmosphere for timescales ranging from decades to millennia, leading to a decrease in atmospheric CO_2 (Kwon et al., 2009; Boyd et al., 2019). Due to the widespread vertical settling behavior of particles in the ocean, their abundance and size not only influence the efficiency of the carbon export but also govern the biogeochemical pathways through which carbon is transformed, remineralized, or permanently stored in the ocean's interior (Kiko et al., 2022). Therefore, the study on distribution characteristics of marine particles, their size composition, and their associated carbon export flux is crucial for gaining a comprehensive understanding of biogeochemical cycles, particularly the carbon cycle in the ocean.

Although marine particles play a crucial role in ocean biogeochemical cycles, their fragile nature poses significant challenges for collection and analysis. Sediment traps have been widely employed to capture settling particles and quantify vertical fluxes (Ramondenc et al., 2016). While this method provides valuable insights, it lacks the spatial coverage and detailed particle size distribution data necessary for a mechanistic understanding of particle dynamics (Wang et al., 2024a). In recent years, advancements in *in situ* optical and imaging technologies have introduced an alternative approach for assessing particle distribution and estimating fluxes (Picheral et al., 2010; Boss et al., 2015). The Underwater Vision Profiler (UVP) has emerged as a powerful tool, enabling high-resolution, *in situ* measurements of particle size distribution and abundance across a broad depth range (Picheral et al., 2010). The compact design of the UVP allows for integration with conductivity, temperature, and depth (CTD) rosette samplers as well as deployment on small autonomous platforms such as underwater gliders (Picheral et al., 2022). When combined with image processing techniques for particle identification, the UVP facilitates comprehensive characterization of particle abundance, size, composition, and potential sources, thereby enhancing our understanding of particle formation and transformation processes. Beyond particle characterization, the UVP has been instrumental in estimating particle fluxes by leveraging

https://doi.org/10.5194/egusphere-2025-2034
Preprint. Discussion started: 27 May 2025
© Author(s) 2025. CC BY 4.0 License.

empirical relationships between particle size and sinking flux (Guidi et al., 2008a; Iversen et al., 2010; Guidi et al., 2016; Ramondenc et al., 2016; Wang et al., 2024b). These flux estimations are derived from *in situ* observations of particle size distributions, where particle abundance is expressed as a function of size (Guidi et al., 2008a; Fender et al., 2019). The high vertical resolution of UVP observations, coupled with established size-dependent relationships for carbon content and sinking velocity (Kriest, 2002; Guidi et al., 2008a; Clements et al., 2023), provides a uniquely detailed perspective on the three-dimensional distribution of particulate organic carbon (POC) flux (Guidi et al., 2016). Observations from the UVP5 have been employed to quantify regional POC fluxes from the surface ocean (Forest et al., 2012; Kiko et al., 2017; Cram et al., 2018) and to reconstruct large-scale carbon export patterns across diverse oceanic biomes (Guidi et al., 2015; Wang et al., 2024b). These advancements underscore the critical role of UVP-based observations in refining our understanding of oceanic carbon cycling and particle-mediated export processes.

The South China Sea (SCS) is one of the largest semi-enclosed marginal seas, characterized by a narrow and steep continental slope in its northern region (Zhang et al., 2020). The northern SCS is influenced by a complex interplay of oceanographic and atmospheric processes, including the monsoon system, frequent typhoons, seasonal intrusions of the Kuroshio Current, and freshwater inputs from the Pearl River (Dai et al., 2020). In addition, mesoscale eddies are frequently observed in the SCS, with Kuroshio Current intrusions playing a dominant role in their formation, particularly in the northern region (Xiu et al., 2010). The continental slope of the SCS serves as a transitional zone between the nutrient- and chlorophyll *a* (Chl *a*) rich shelf waters and the oligotrophic open ocean, playing a crucial role in regulating material and energy exchange between these two systems (Zhang et al., 2023). This slope features a rapid bathymetric gradient, with depths increasing sharply from less than 200 m at the shelf break to over 1000 m. The region is influenced by multiple water masses, including Kuroshio intrusions, a southwestward along-slope current, and cross-slope transport of fresher water originating from the Pearl River (Wang et al., 2019). These unique hydrographic conditions exert complex influence on the production, aggregation, and sinking of marine particles (Turner et al., 2017), making the region a critical yet underexplored area for understanding particle-mediated carbon export.

Several studies have investigated particle export fluxes in the SCS. Li et al. (2017) analyzed POC sinking fluxes at a depth of 1200 m in the central SCS using a seven-year time series of sediment trap observations, revealing that the East Asian Monsoon and mesoscale eddies jointly regulate POC flux variability. Zhou et al. (2020) examined the temporal variations in ^{234}Th-based particle export from 2004 to 2014 at the South-East Asian Time-series Study (SEATS) site and found that particle flux increased with mixed layer depth, particularly in winter, due to the influence of the strong northeast monsoon. Hong et al. (2021) quantified cross-shelf POC export in the northern SCS shelf using ^{234}Th-based estimates and sediment traps, reporting a vertical POC flux of 26 mmol m^{-2} d^{-1} from the euphotic zone and a cross-shelf transport flux of 9.9 mmol m^{-2} d^{-1}. Ma et al. (2023) investigated nutrient-dependent export productivity structures within the euphotic zone of the oligotrophic SCS basin, highlighting that even the nutrient-depleted layer can act as a net exporter of POC. Despite these valuable contributions, most previous studies have relied on sediment traps or radionuclide-based methods, which provide limited information on the size structure and vertical evolution of particle fluxes. In particular, *in situ*, size-resolved observations that link particle abundance, size composition, and export efficiency under dynamic physical forcing (e.g., eddies) remain scarce in the SCS slope region. This lack of direct observational constraints hampers our ability to evaluate the role of particle size in modulating carbon export pathways and their sensitivity to mesoscale variability.

https://doi.org/10.5194/egusphere-2025-2034
Preprint. Discussion started: 27 May 2025
© Author(s) 2025. CC BY 4.0 License.

This study aims to address these knowledge gaps by analyzing high-resolution UVP data collected from the continental slope of the SCS during a 2015 survey, during which an anticyclonic-cyclonic eddy pair was observed. Specifically, our objectives are to (1) characterize the spatial distribution patterns of marine particles, both horizontally and vertically, (2) quantify the POC flux associated with particle sedimentation and compare the relative contributions of particles with different sizes, and (3) investigate the influence of mesoscale eddies on particle dynamics and carbon export processes in this region. Unlike previous studies that primarily focused on surface-derived carbon fluxes or bulk particle inventories, this study integrates size-resolved, *in situ* particle observations with empirical flux estimates to examine depth-dependent export processes along a dynamic continental slope. These findings contribute to a better understanding of the spatial heterogeneity and controlling factors of the biological pump in the SCS, and offer process-level observational constraints that can inform carbon flux modeling in other oligotrophic slope systems.

2 Material and methods

2.1 Surveyed area and data acquisition

A research cruise was carried out in the SCS aboard the research vessel *Nanfeng* from June 13 to June 29, 2015. The study area and survey stations were shown in Fig. 1a. The survey stations can be divided into three transects (Transect 1, Transect 2, and Transect 3) (Fig. 1b), which extend across the slope of the SCS, with shallower sites at over 100 m and deeper sites exceeding 1000 m in depth (Table 1). Satellite data were used to analyze the spatial and temporal variations in the physical and dynamic characteristics of the study region. The Sea Surface Salinity (SSS) data consists of daily global, gap-free Level-4 (L4) analyses of SSS at a resolution of 1/8°. These analyses are generated through a multivariate optimal interpolation algorithm that combines SSS data from different satellite sources, including NASA's Soil Moisture Active Passive (SMAP) and ESA'S Soil Moisture Ocean Salinity (SMOS) satellites, along with *in situ* salinity measurements provided by the Copernicus Marine Environment Monitoring Service (Multi Observation Global Ocean Sea Surface Salinity and Sea Surface Density). Eddies were identified as local minima (cyclonic eddies) and maxima (anticyclonic eddies) in sea level anomaly (SLA) using a composite altimetry product, which is based on a combination of remote sensing observations distributed by the Copernicus Marine Environment Monitoring Service (SEALEVEL_GLO_PHY_CLIMATE_L4_MY_008_057).

https://doi.org/10.5194/egusphere-2025-2034
Preprint. Discussion started: 27 May 2025
© Author(s) 2025. CC BY 4.0 License.

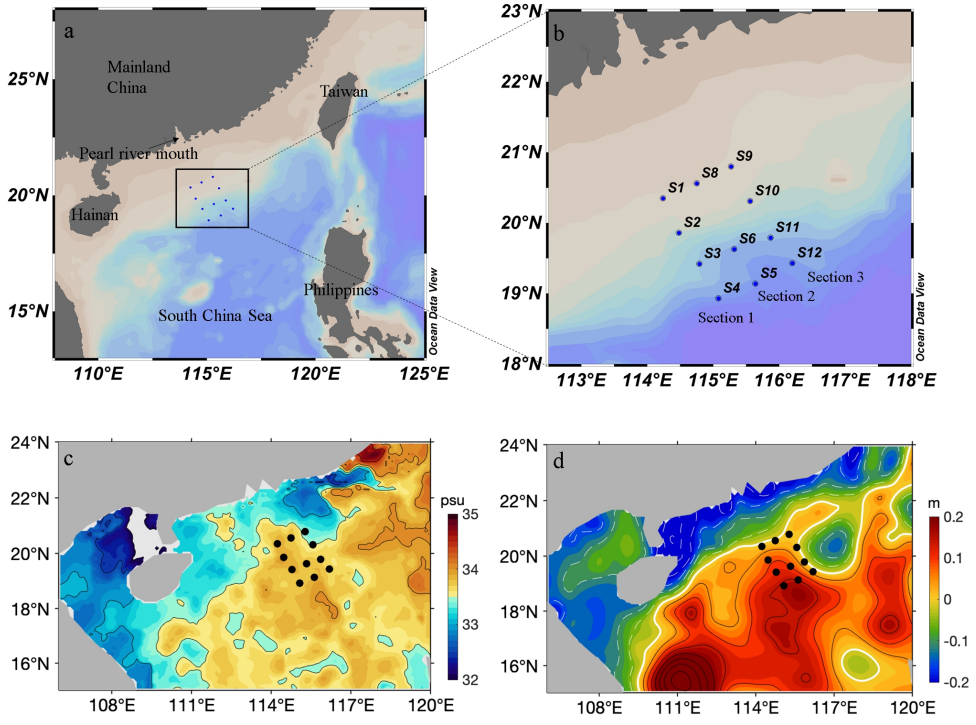

Fig. 1 Study area and survey stations in the SCS continental slope. a: the study region; b: the enlarge view; c: sea surface salinity (SSS) at 1/8° of resolution; d: sea level anomalies (SLA). The dots indicate the locations of the sampling stations.

https://doi.org/10.5194/egusphere-2025-2034
Preprint. Discussion started: 27 May 2025
© Author(s) 2025. CC BY 4.0 License.

Table 1. Location and deployment times of UVP in the study area.

Station	Longitude	Latitude	Date	Time	Bottom depth (m)	UVP deployment depth (m)
S1	114.40	20.29	18-June-2015	02:40 p.m.	123	110
S2	114.47	19.87	17-June-2015	03:45 a.m.	587	500
S3	114.79	19.42	16-June-2015	01:35 p.m.	1300	800
S4	115.08	18.93	15-June-2015	11:45 p.m.	3000	800
S5	115.64	19.14	15-June-2015	07:30 a.m.	2800	800
S6	115.32	19.63	14-June-2015	03:25 p.m.	2108	800
S8	114.75	20.56	18-June-2015	08:50 p.m.	120	100
S9	115.27	20.80	19-June-2015	08:15 a.m.	170	110
S10	115.56	20.31	19-June-2015	07:30 p.m.	560	500
S11	115.86	19.78	20-June-2015	01:20 p.m.	1556	800
S12	116.20	19.43	21-June-2015	01:45 p.m.	1971	800

Hydrographic measurements and water sampling were conducted using an SBE911 plus dual conductivity-temperature-depth (CTD) sensor unit coupled with an SBE 32 Water Sampler (Seabird Scientific, Bellevue, WA, USA). The CTD system recorded temperature, salinity, and pressure profiles throughout the water column.

Nutrients and chlorophyll *a* (Chl *a*) concentrations were determined from seawater samples collected at multiple depths using a 10 L Niskin sampler (KC-Denmark Inc., Denmark) deployed alongside a CTD. For nutrient analysis, seawater samples were filtered through a 0.45 μm pore-size cellulose acetate membrane, and the filtrates were stored at temperatures below -20 ℃ until further processing. In the laboratory, nutrient concentrations were measured using a Technicon AA3 autoanalyzer (Bran-Luebbe GmbH) following standard protocols (Liu et al., 2022). The detection limits for nutrient analysis were 0.02 μmol L^{-1} for NO_3^-, 0.01 μmol L^{-1} for NO_2^-, 0.03 μmol L^{-1} for PO_4^{3-}, and 0.05 μmol L^{-1} for SiO_3^{2-}. Chl *a* concentrations were determined using the fluorometric method (Welschmeyer, 1994). Seawater samples (500 mL) were filtered through 0.7 μm Whatman GF/F filters, and pigments were extracted in 90% acetone at 4 ℃ in the dark for 24 h. Fluorescence measurements were then conducted using a Turner Designs fluorometer (Model 10).

2.2 Particle measurement

Particle size and abundance were measured using a high-resolution, high-frequency Underwater Vision Profiler (UVP 5.0). The UVP was mounted downward-facing on the CTD Niskin-rosette, and

https://doi.org/10.5194/egusphere-2025-2034
Preprint. Discussion started: 27 May 2025
© Author(s) 2025. CC BY 4.0 License.

vertical deployments were conducted at a descent speed of 1 m/s. The UVP captured images of illuminated particles within a known sampling volume of 10.53 L. Particle size was determined based on the number of pixels in the captured images. Size and volume calibrations were performed in a seawater tank using natural particles of various types to establish the pixel-to-metric unit conversion (Picheral et al., 2010). Images were recorded digitally at a rate of 12 frames per second and processed using custom developed image analysis software. The equivalent spherical diameter (ESD) of each particle was calculated under the assumption that the particle's projected shape was circular. Particle volume concentration (PVC) was calculated by summing the estimated volumes of all particles detected within each depth bin and normalizing by the corresponding sampled water volume. The volume of each particle was estimated by assuming spherical geometry based on the ESD. The final PVC is reported in $mm^3\ L^{-1}$.

Previous inter-calibration studies of UVP systems have shown that only the overlapping size ranges among different studies are suitable for comparative particle profile analyses (Guidi et al., 2008a; Picheral et al., 2010). For consistency with previous studies, we set the upper size limit for particle flux calculations at 1.5 mm (Guidi et al., 2007, 2008a; Stemmann et al., 2008; Ramondenc et al., 2016). The lower size limit was set at 100 µm to exclude signals potentially caused by camera resolution constraints and background noise, which could not be reliably distinguished as actual particles (Fender et al. 2019). For data visualization in this study, particle abundance was categorized following Kiko et al. (2022) into two groups: small particles (ESD < 0.50 mm) and large particles (ESD ≥ 0.50 mm). This classification provides insights into size-dependent particle dynamics, including aggregation, disaggregation, and vertical transport processes.

2.3 Estimation of POC export flux from particle size spectrum

The POC export flux was estimated from particle size spectra using the method developed by Guidi et al. (2008a, b). The particle size distribution (PSD) generally follows a power-law decrease over the µm to mm size range (Guidi et al., 2009). This distribution, derived from UVP images, is expressed as:

$$n(d) = \alpha d^{\beta} \quad (1)$$

where d (mm) represents particles diameter, $n(d)$ is the particle size spectrum, α is normalization constant and β is the exponent characterizing the slope of the number spectrum after log transformation.

https://doi.org/10.5194/egusphere-2025-2034
Preprint. Discussion started: 27 May 2025
© Author(s) 2025. CC BY 4.0 License.

The particle size-based carbon flux approach assumes that the total carbon flux (F) (mg C m^{-2} d^{-1}) corresponds to the integration of the flux spectrum over all particle sizes, from the smallest (d_{min}) to the largest (d_{max}) particle size:

$$F = \int_{d_{min}}^{d_{max}} n(d) \cdot m(d) \cdot w(d) dd \quad (2)$$

where $m(d)$ (mg C) represents the mass (carbon content) of a spherical particle, and $w(d)$ (m d^{-1}) is its sinking velocity, estimated using Stokes' Law.

The combined particle mass and settling velocity follow a power-law function of particle diameter, based on empirical relationships derived from comparisons of PSDs obtained through imaging systems and sediment trap mass flux estimates (Guidi et al., 2008a; Jouandet et al., 2011). This relationship is expressed as: $m(d) \cdot w(d) = Ad^B$, where A (mg C m d^{-1}) and B are empirical constants. The particle carbon flux can thus be approximated by discretizing Equation (2) into small logarithmic diameter intervals (Guidi et al., 2009; Picheral et al., 2010):

$$F = \sum_{i=1}^{x} n_i A d_i^B \Delta d_i \quad (3)$$

where A = 12.5 ± 3.40 and B = 3.81 ± 0.70, representing the best-fit parameters that minimized log-transformed discrepancies between global oceanic sediment trap-derived carbon flux estimates and UVP-derived particle abundance and PSDs (Guidi et al., 2008a). This approach has been widely applied in various oceanic regions worldwide in recent years (Iversen et al., 2010; Ramondenc et al., 2016; Fender et al., 2019; Clements et al., 2023; Wang et al., 2024a, b).

2.4 Data analysis

All particle size and abundance data obtained from the UVP were binned into 5 m vertical intervals and subsequently processed to generate depth profiles of particle abundance, particle volume concentration, and POC flux. Statistical analyses were performed using SPSS 25.0. Two-tailed independent-sample t-tests were conducted to assess significant differences in particle and flux parameters between different depth layers and regions. Prior to applying t-tests, data normality and variance homogeneity were tested using the Shapiro-Wilk and Levene's tests, respectively. For data not meeting parametric assumptions, non-parametric alternatives were used. Pearson correlation analysis (PCA) was applied to evaluate the relationships between POC flux and environmental variables. Significance was defined at $p < 0.05$ unless otherwise stated. Hydrographic and particle data were visualized using Ocean Data View 4 and Origin 2022.

https://doi.org/10.5194/egusphere-2025-2034
Preprint. Discussion started: 27 May 2025
© Author(s) 2025. CC BY 4.0 License.

3 Results

3.1 Hydrographic conditions

Based on the spatial distribution of SLA, two mesoscale eddies were present in the study area during the survey period: one cyclonic eddy and one anticyclonic eddy (Fig. 1d). The outer stations of Transects 1 and 2, S4 and S5, were influenced by the anticyclonic eddy, whereas stations S11 and S12 in Transect 3 were located at the periphery of the cyclonic eddy. Based on the distribution of sea surface salinity (SSS) (Fig. 1c), the salinity at stations S9 and S10 along Transect 3 was lower than at other stations. In situ CTD measurements further confirmed that the upper water column at these stations exhibited reduced salinity (Supplementary Fig. S1f), indicating a certain degree of influence from the Pearl River plume. Vertically, the study area exhibits distinct characteristics of a tropical ocean, with relatively high sea surface temperature (~30 °C) and strong stratification in the upper 200 m (Fig. 2). A pronounced thermocline is observed between 100 and 200 m, marking a sharp temperature gradient (Fig. 2a, c and e). Salinity increases with depth, further reinforcing the stratification pattern (Fig. 2b, d and f).

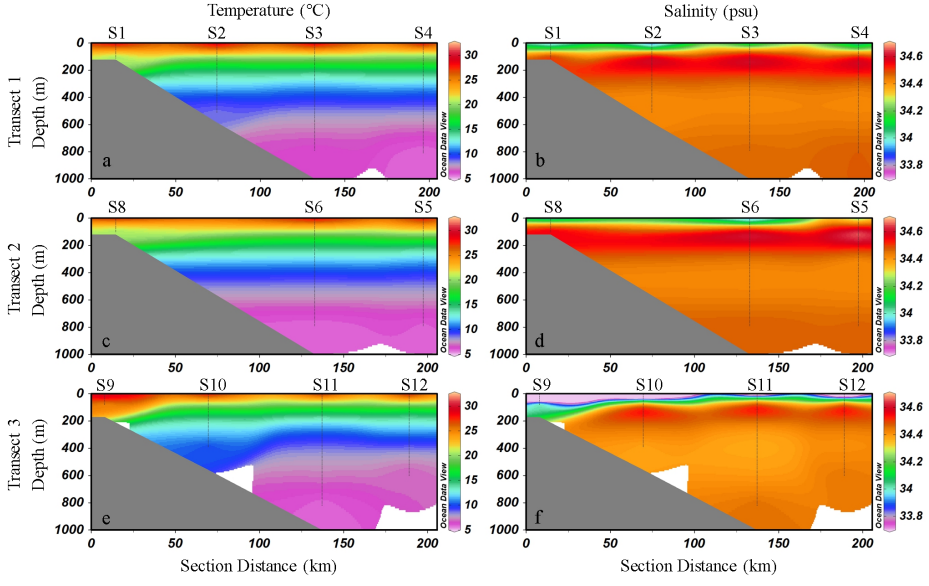

Fig. 2. Vertical distribution of temperature (°C) and salinity (psu) along the three transects in the study area. Transect 1: temperature (a, °C), salinity (b, psu); Transect 2: temperature (c, °C), salinity (d, psu); Transect

https://doi.org/10.5194/egusphere-2025-2034
Preprint. Discussion started: 27 May 2025
© Author(s) 2025. CC BY 4.0 License.

3: temperature (e, ℃), salinity (f, psu)

The sectional distributions of nutrients in the study area are presented in Fig. 3. The nutrient distribution follows the typical characteristics of tropical oligotrophic waters, with low nutrient concentrations in the upper water column and a pronounced nutricline occurring between 50 and 100 m, where nutrient concentrations increase sharply (Fig. 3). At most stations, surface nitrate concentrations were below the detection limit, except for Transect 3. At the inner station of Transect 3 (S9), the surface nitrate concentration was 2.3 μmol L^{-1}. The outer stations of Transect 3, S11 and S12, exhibited surface nitrate concentrations of 2.8 μmol L^{-1} and 1.33 μmol L^{-1}, respectively. These values were significantly higher than those observed at surface waters of Transects 1 and 2 (*t*-test, $p < 0.01$), where nitrate concentrations generally remained below 0.1 μmol L^{-1} (Fig. 3a, d). Phosphate and silicate exhibit distribution patterns similar to those of nitrate. The concentrations of nitrate and phosphate in the upper 50 m were generally higher at the cyclonic eddy stations (S11, S12) compared to the anticyclonic eddy stations (S4, S5) (*t*-test, $p < 0.01$), and silicate concentrations were relatively consistent across these stations (Supplementary Fig. S2).

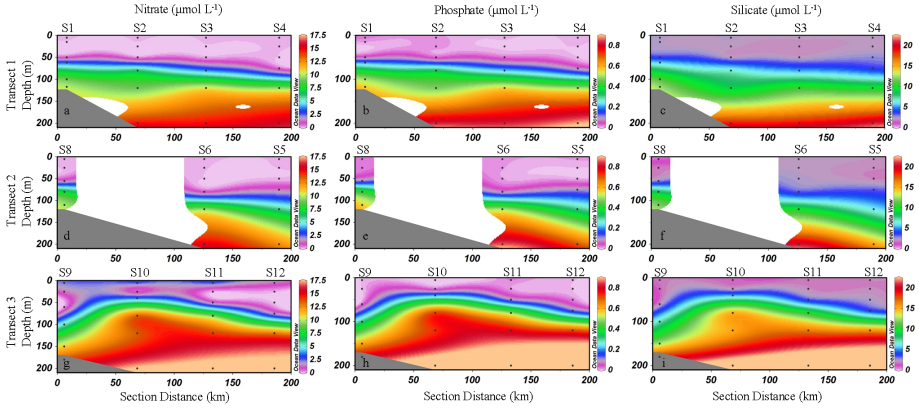

Fig. 3. Sectional distribution of nutrient concentrations (nitrate, phosphate, and silicate) (μmol L^{-1}) in the upper 200 m of the study area. Transect 1: nitrate (a, μmol L^{-1}), phosphate (b, μmol L^{-1}), silicate (c, μmol L^{-1}); Transect 2: nitrate (d, μmol L^{-1}), phosphate (e, μmol L^{-1}), silicate (f, μmol L^{-1}); Transect 3: nitrate (g, μmol L^{-1}), phosphate (h, μmol L^{-1}), silicate (i, μmol L^{-1})

https://doi.org/10.5194/egusphere-2025-2034
Preprint. Discussion started: 27 May 2025
© Author(s) 2025. CC BY 4.0 License.

The sectional profiles of Chl *a* concentration reveal significant spatial variability in primary productivity across the study area (Fig. 4). In Transect 1, a pronounced subsurface chlorophyll maximum (SCM) is observed at approximately 50–100 m depth, particularly near the coastal stations, where Chl *a* concentrations exceed 0.6 μg L^{-1} (Fig. 4a). In Transect 2, the SCM is most prominent at the nearshore station, where the highest Chl *a* concentration of 1.6 μg L^{-1} occurs around 50 m depth. As the transect extends offshore, the SCM becomes less pronounced, with peak Chl *a* concentrations ranging from 0.2 to 0.4 μg L^{-1}. In Transect 3, relatively high Chl *a* concentrations are observed in the upper 50 m at the nearshore station (Fig. 4c). Further offshore, Chl *a* concentrations decrease, forming a well-defined SCM. At the outermost station, relatively elevated Chl *a* concentrations persist in the upper 50 m. The Chl *a* concentrations in the upper 50 m at the cyclonic eddy-influenced stations S11 and S12 were higher than those at the anticyclonic eddy-influenced stations S4 and S5 (Supplementary Fig. S2d).

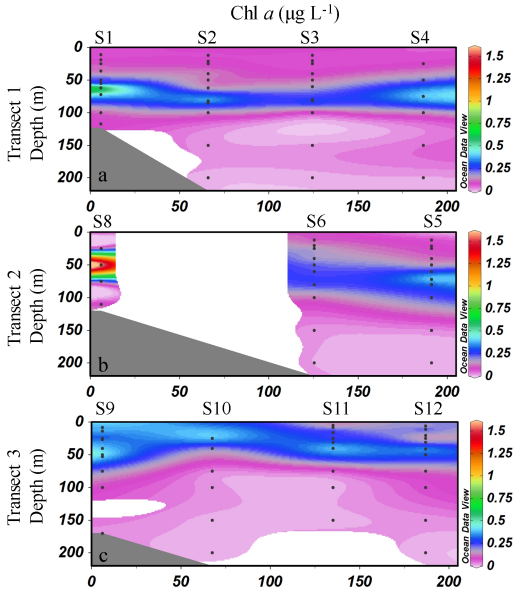

Fig. 4. Sectional distributions of Chl *a* (μg L^{-1}) along the three transects in the study area. a: Transect 1; b: Transect 2; c: Transect 3

3.2 Particle concentration and distribution

Particle abundances ranged from 0 to 783 particles L^{-1} with a mean of 68 ± 68 particles L^{-1}. The vertical profiles of particle abundance across the three transects exhibited distinct spatial and depth-related variations (Fig. 5). In Transect 1, high particle abundance was observed in the bottom waters of the nearshore station S1 and the slope station S2, with values reaching up to 700 particles L^{-1} at 500 m depth at station S2 (Fig. 5a). Notably, the vast majority of particles at this depth were small particles (ESD < 500 μm), accounting for over 99% of the total particle abundance (Fig. 5b). Additionally, a slight increase in particle abundance was observed in the 60–80 m layer at the outer slope station S4. In Transect 2, particle abundance gradually decreased from the inner shelf to the outer slope and from surface to bottom waters (Fig. 5d). In Transect 3, a distinct peak in particle abundance was observed at 379–390 m depth at the slope station S10 (Fig. 5g). Furthermore, at the

https://doi.org/10.5194/egusphere-2025-2034
Preprint. Discussion started: 27 May 2025
© Author(s) 2025. CC BY 4.0 License.

outermost stations S11 and S12, elevated particle concentrations were observed in the upper 50 m of the water column, with peak values reaching up to 200 particles L^{-1}. This is significantly higher than the maximum particle abundances recorded at stations station S4 and S5, where values remained below 150 particles L^{-1} (Fig. 5a, d). Regarding particle size composition, small particles overwhelmingly dominated the total particle abundance, consistently accounting for more than 97% across all transects and throughout the water column (Fig. 5b, e, h). In contrast, large particles contributed only a minor fraction of the total abundance at all depths and locations (Fig. 5c, f, i), highlighting the numerical dominance of small particles in the study area.

Particle volume concentration (PVC) ranged from 0 to 6.7 mm^3 L^{-1}, with a mean of 0.3 ± 0.4 mm^3 L^{-1}. The overall distribution of PVC across the three transects generally aligns with the patterns observed in particle abundance but exhibits some notable differences (Fig. 6). In Transect 1, PVC was highest at the inner slope station S1 and progressively decreased toward the outer slope stations (Fig. 6a). A similar pattern was observed in Transect 2, where PVC was elevated at the inner slope station S8, followed by a gradual decline toward the outer slope (Fig. 6d). In Transect 3, PVC was relatively high in the upper 70 m at the outermost stations S11 and S12, with concentrations decreasing with depth (Fig. 6g). Notably, despite the high particle abundance observed in the deep waters at stations S2 and S10, PVC in these layers remained low (Fig. 6a, g). This discrepancy suggests that the high particle abundance in these regions was primarily driven by small particles, which contributed minimally to the overall particle volume. In contrast, at stations S11 and S12, the PVC distribution closely followed the particle abundance pattern, with elevated concentrations reaching up to 1.2 mm^3 L^{-1} in the upper water column. Representative particle images captured by the UVP in the upper layers at stations S11 and S12 are shown in Fig. 7. For the whole study region, small particles contribute between 13% and 74% (mean = 39% ± 12%) of the total PVC, while large particles account for 26% to 87% (mean = 61% ± 12%). Unlike their overwhelming dominance in particle abundance, small particles no longer play a predominant role in PVC. Instead, large particles contribute a greater proportion to PVC, emphasizing their larger size and greater volumetric influence despite their low numerical abundance.

Particle abundance and PVC showed clear spatial differences between the cyclonic and anticyclonic eddy regions (Fig. S3). At the anticyclonic eddy stations (S4 and S5), particle abundance remained low in the upper 50 m layer, averaging 51 particles L^{-1}, and PVC values were also limited, generally less than 0.3 mm^3 L^{-1}. In contrast, the cyclonic eddy stations (S11 and S12) exhibited significantly higher values for both parameters. Particle abundance at these stations exceeded 120 particles L^{-1}, and PVC increased markedly under the influence of cyclonic eddies, with values exceeding 0.6 mm^3 L^{-1}.

https://doi.org/10.5194/egusphere-2025-2034
Preprint. Discussion started: 27 May 2025
© Author(s) 2025. CC BY 4.0 License.

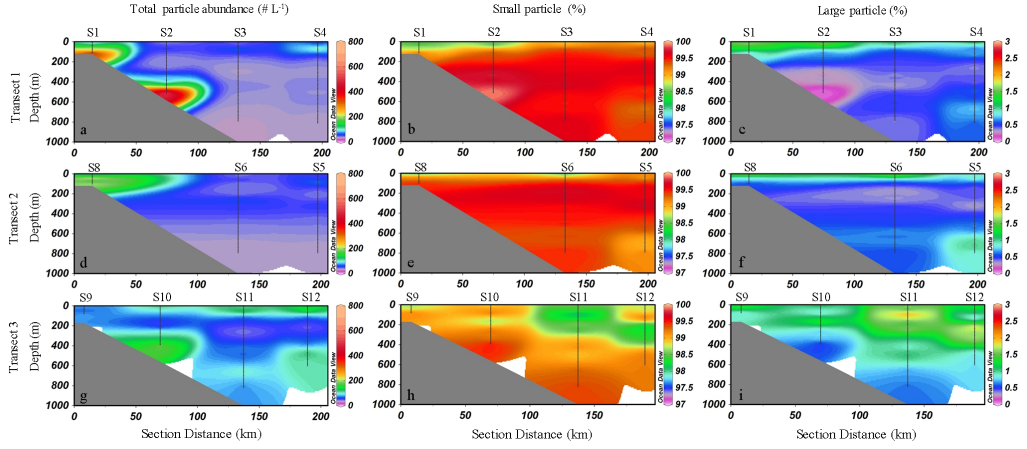

Fig. 5. Vertical distribution of particles abundance (# L^{-1}) and the relative proportion of small particles (ESD < 500 µm) and large particles (ESD ≥ 500 µm) within the total particle abundance. Transect 1: particle abundance (a, # L^{-1}), small particles (%) (b), large particles (%) (c); Transect 2: particle abundance (d, # L^{-1}), small particles (%) (e), large particles (%) (f); Transect 3: particle abundance (g, # L^{-1}), small particles (%) (h), large particles (%) (i)

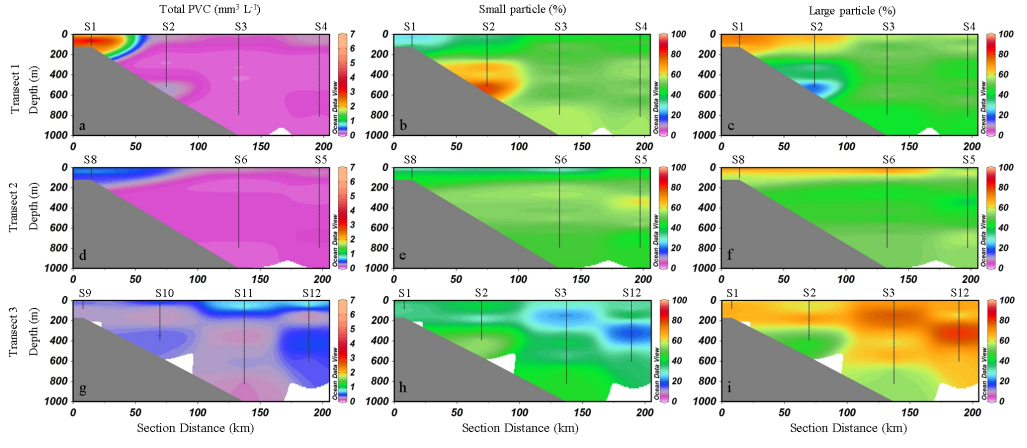

Fig. 6. Vertical distribution of particle volume concentration (PVC) (mm^3 L^{-1}) and the relative contribution of small particles (ESD < 500 µm) and large particles (ESD ≥ 500 µm) to the total PVC. Transect 1: PVC (a, mm^3 L^{-1}), small particles (%) (b), large particles (%) (c); Transect 2: PVC (d, mm^3 L^{-1}), small particles (%) (e), large particles (%) (f); Transect 3: PVC (g, mm^3 L^{-1}), small particles (%) (h), large particles (%) (i)

https://doi.org/10.5194/egusphere-2025-2034
Preprint. Discussion started: 27 May 2025
© Author(s) 2025. CC BY 4.0 License.

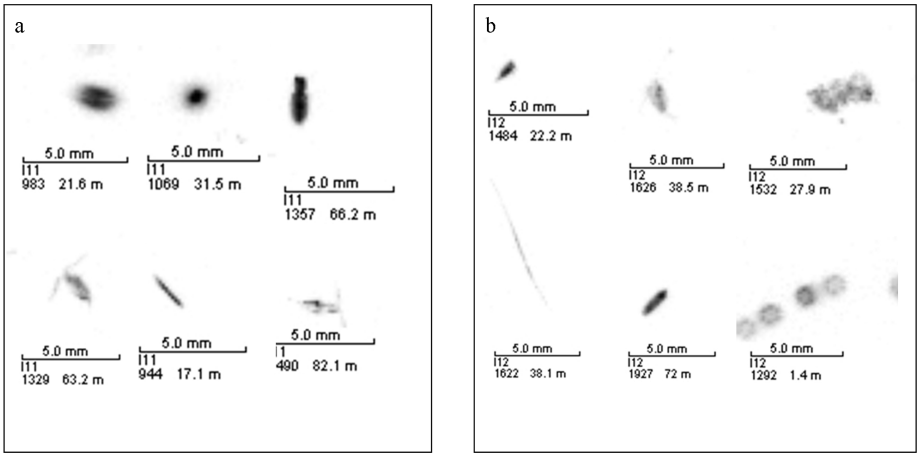

Fig. 7. Representative images of large particles captured by the UVP at station S11 and S12. a: S11; b: S12. Scale bar represents 5 mm. Each image includes the station name, image number, and the depth at which it was taken.

Vertically, the mean particle abundance and PVC in waters shallower than 200 m were 79 ± 70 particles L^{-1} and 0.4 ± 0.7 mm^3 L^{-1}, respectively, which were significantly higher than those in waters deeper than 200 m, with mean values of 59 ± 66 particles L^{-1} and 0.2 ± 0.1 mm^3 L^{-1} (*t*-test, $p < 0.01$) (Supplementary Fig. S4). This indicates that, overall, particle abundance and PVC are higher in the upper 200 m zone compared to deeper waters.

3.3 POC export flux and spatial variability

The POC export flux, derived from UVP-based particle size distributions, exhibited a wide range from 3.4 to 302.4 mg C m^{-2} d^{-1}, with a mean value of 33.6 ± 34.9 mg C m^{-2} d^{-1} across the study area. Notable spatial heterogeneity was observed both within and between transects (Fig. 8), reflecting the combined influence of productivity gradients, hydrodynamic structure, and particle aggregation dynamics. In Transect 1, the highest fluxes were concentrated at the nearshore station S1, particularly within the 50–70 m depth range, where values peaked at 302.0 mg C m^{-2} d^{-1} (Fig. 8a). In contrast, offshore stations along the same transect displayed significantly lower fluxes, generally below 40 mg C m^{-2} d^{-1}, indicating a strong coastal-to-offshore decline driven by reduced primary production and weaker aggregation processes. A similar nearshore-to-offshore gradient was observed in Transect 2, where the maximum flux (164.0 mg C m^{-2} d^{-1}) was recorded at 40 m depth at station S8, gradually decreasing toward deeper slope stations (Fig. 8b). Transect 3 showed a distinct pattern, with elevated POC fluxes occurring at offshore stations S11 and S12 (Fig. 8c). At station S11, the highest flux (212 mg C m^{-2} d^{-1}) was recorded at 60 m, while at station S12, the flux peaked at 210 mg C m^{-2} d^{-1} at 40 m. Moreover, POC fluxes at depths of 200–600 m at stations S11 and S12 remained substantially higher than those at comparable depths in the offshore stations of Transects 1 and 2 (Fig. 8a, b), implying sustained vertical transfer of organic material.

https://doi.org/10.5194/egusphere-2025-2034
Preprint. Discussion started: 27 May 2025
© Author(s) 2025. CC BY 4.0 License.

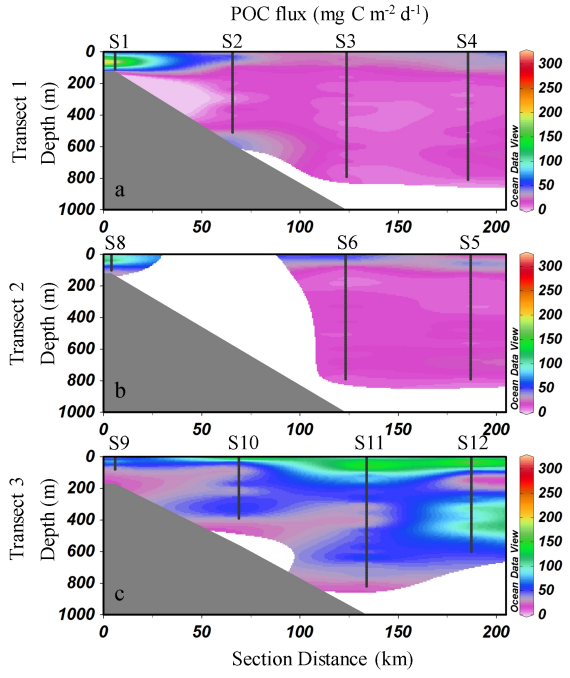

Fig. 8 Vertical distribution of POC flux across the three transects (mg C m^{-2} d^{-1}) in the study area. a: Transect 1; b: Transect 2; c: Transect 3

POC fluxes exhibited pronounced spatial and vertical variability between the cyclonic eddy-influenced and anticyclonic eddy-influenced regions (Fig. 9). At the upper layers (50 m and 100 m), POC fluxes were substantially higher at the cyclonic eddy stations (S11 and S12), with maximum values exceeding 100 mg C m^{-2} d^{-1}. In contrast, the anticyclonic eddy stations (S4 and S5) exhibited much lower fluxes, generally below 60 mg C m^{-2} d^{-1} (Fig. 9a, b). At 200 m, this pattern persisted, with S11 maintaining the highest flux, while S4 and S5 showed sharp decreases to below 30 mg C m^{-2} d^{-1}, indicating limited vertical export in the anticyclonic eddy region (Fig. 9c). Deeper layers (400 m and 600 m) also demonstrated elevated fluxes at the cyclonic eddy stations, especially S12, where fluxes remained above 60 mg C m^{-2} d^{-1}. Meanwhile, fluxes at S4 and S5 were consistently low across all depths, with values typically below 30 mg C m^{-2} d^{-1} (Fig. 9d, e).

https://doi.org/10.5194/egusphere-2025-2034
Preprint. Discussion started: 27 May 2025
© Author(s) 2025. CC BY 4.0 License.

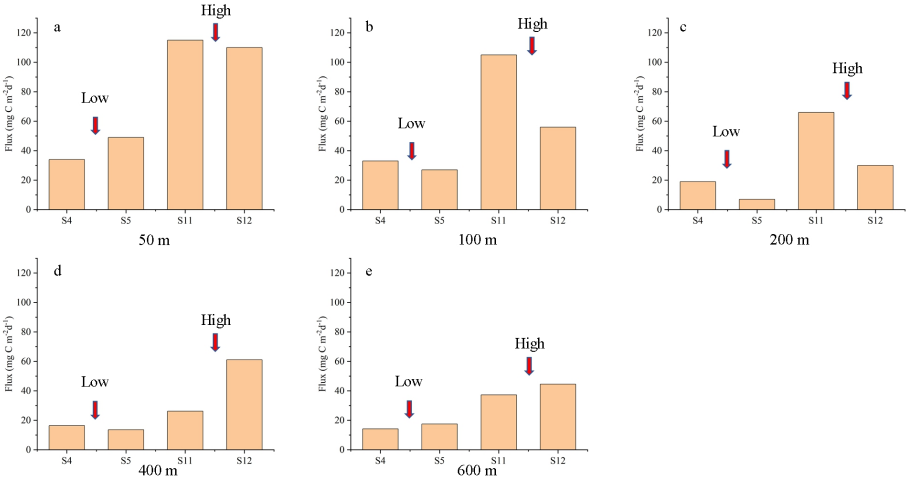

Fig. 9 POC flux derived from UVP data in different water layers at stations located in the anticyclonic eddy region (S4, S5) and cyclonic eddy region (S11, S12). a: 50 m; b: 100 m; c: 200 m; d: 400 m; e: 600 m.

The contribution of small and large particles to POC flux exhibits considerable variability across the study area (Fig. 10). Small particle-derived carbon flux accounted for 5.1% to 76.7% of the total POC flux, with an average contribution of 23.8% ± 11.5%, while large particle-derived carbon flux ranged from 23.3% to 95.0%, averaging 76.2% ± 11.5%. These results indicate that POC export flux in the study area is primarily driven by the sedimentation of large particles (ESD ≥ 500 μm). A few exceptions are noteworthy. At 500 m depth at station S2, small particles contributed more than 50% of the POC flux (Fig. 10a), while at 380 m depth at station S10, small particles accounted for over 30% of the POC flux (Fig. 10e), significantly higher than in other regions. In contrast, in the 200–600 m depth range at stations S11 and S12, the contribution of large particles to POC flux significantly increased, with an average proportion of 87% (Fig. 10f). This proportion was notably higher than that in the same depth range at the offshore stations of Transects 1 and 2, where large particles accounted for 71% and 68% of the POC flux, respectively (Fig. 10b, d). The increased dominance of large particles at depth in Transect 3 suggests more efficient transport of larger aggregates, potentially influenced by mesoscale eddies or enhanced particle formation and retention processes.

https://doi.org/10.5194/egusphere-2025-2034
Preprint. Discussion started: 27 May 2025
© Author(s) 2025. CC BY 4.0 License.

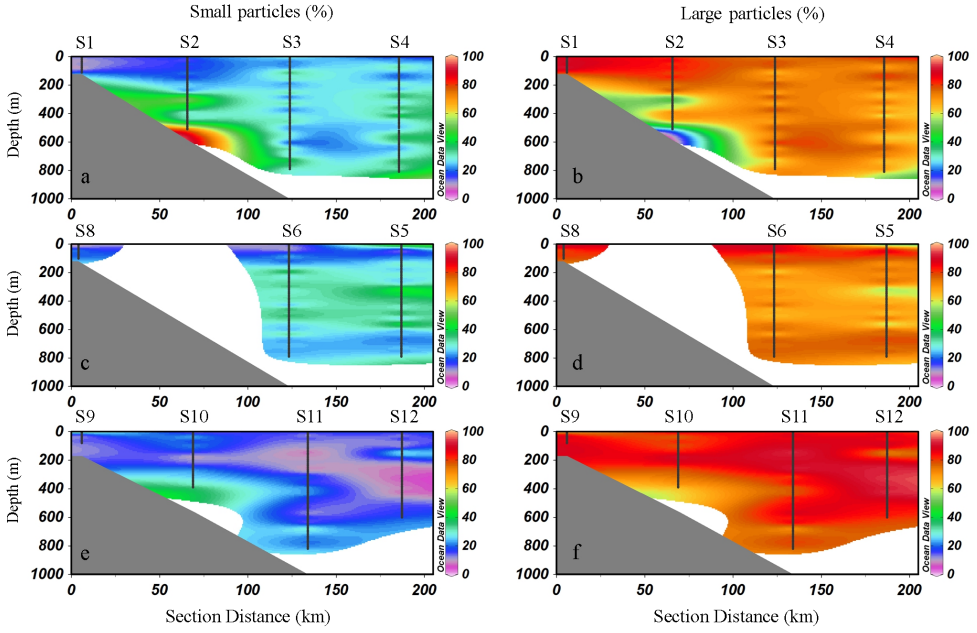

Fig. 10 Contribution of small and large particles to the POC flux across the three transects in the study area. Transect 1: a, small particles (%); b, large particles (%). Transect 2: c, small particles (%); d, large particles (%). Transect 3: e, small particles (%); f, large particles (%).

Vertically, high POC export flux values are predominantly observed within the upper 100 m, with peak concentrations around the 50 m depth layer (Fig. 11a). Below 100 m, the flux generally exhibits a decreasing trend with increasing depth. This pattern is consistent for both small and large particles, as their respective carbon flux distributions follow a similar trend (Fig. 11b, c). However, the percentage contributions of small and large particles to the total POC flux exhibited distinct vertical patterns. Specifically, the relative contribution of small particles generally increased with depth, while that of large particles showed a decreasing trend (Supplementary Fig. S5).

https://doi.org/10.5194/egusphere-2025-2034
Preprint. Discussion started: 27 May 2025
© Author(s) 2025. CC BY 4.0 License.

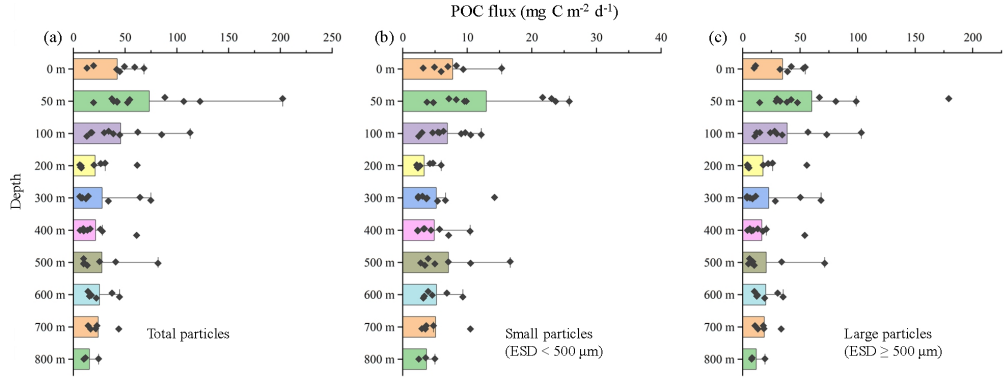

Fig. 11 Vertical distributions of POC export flux (mg C m^{-2} d^{-1}) in different layers in the study area. a: total POC export flux; b: export flux of small particles (ESD < 500 μm); c: export flux of large particles (ESD ≥ 500 μm). Box plots show the median value (mid-line), the 25% and 75% quantiles (box), and the 5 and 95% quantiles (whiskers).

3.4 Correlation analysis

The results of the PCA correlation analysis indicate that above 200 m, POC flux does not exhibit significant correlations with most environmental factors, except for water depth and Chl *a* concentration (Fig. 12a). POC flux shows a significant negative correlation with water depth and a significant positive correlation with Chl *a* concentration. In addition to the correlation matrix, scatter plot analyses further revealed significant positive relationships between POC flux at 200 m, 400 m, and 600 m depths and the water-column integrated Chl *a* concentrations above 200 m (Fig. 12b-d). The strength of correlation remained consistent across these depth layers, indicating that surface phytoplankton biomass is a key determinant of vertical carbon flux throughout the upper to mid-mesopelagic zone. These results suggest a tight coupling between surface production and deep particle export. Scatter plot analysis across the full water column revealed contrasting relationships between POC flux and the abundance of small and large particles (Fig. 13). No significant correlation was found between POC flux and small particles (Fig.13a), suggesting that variations in the abundance of small particles alone are not reliable indicators of vertical carbon export. In contrast, POC flux showed a significant positive linear correlation with large particle abundance (Fig. 13b), with a fitted regression equation of $y = 48.63x - 3.27$ ($p < 0.05$). This pattern underscores the dominant role of large particles in mediating efficient vertical carbon transfer.

https://doi.org/10.5194/egusphere-2025-2034
Preprint. Discussion started: 27 May 2025
© Author(s) 2025. CC BY 4.0 License.

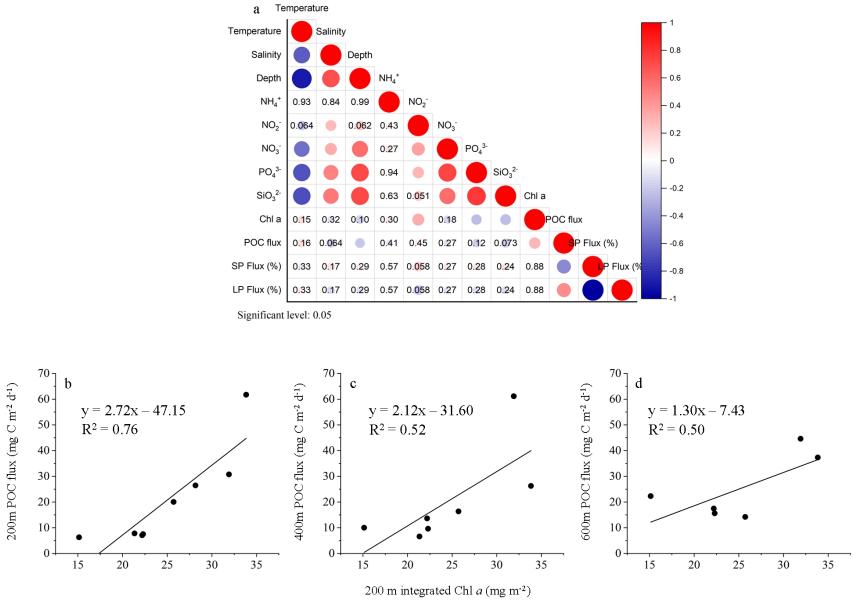

Fig. 12 Correlation analysis between POC flux and environmental factors.

a: Heatmap of Pearson Correlation Analysis between POC flux in the upper 200 m and environmental factors; b-d: Correlation between POC (mg C m^{-2} d^{-1}) flux at 200 m, 400 m, and 600 m depth and the integrated Chl *a* concentration (mg m^{-2}) in the upper 200m. SP: small particle; LP: large particle.

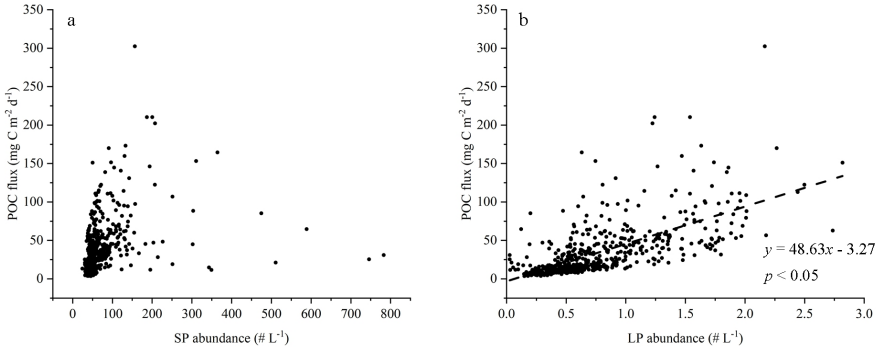

Fig. 13 Scatter plots of POC flux versus abundance of small particles (a) and large particles (b). SP: small particle; LP: large particle. *p* represents the PCA correlation coefficient, and $p < 0.05$ indicates a significant correlation between the two datasets.

4 Discussion

4.1 Comparison of particle abundance and volume concentration with other oceanic regions

The particle abundance and volume concentration (PVC) observed with UVP along the continental slope of

https://doi.org/10.5194/egusphere-2025-2034
Preprint. Discussion started: 27 May 2025
© Author(s) 2025. CC BY 4.0 License.

the SCS in this study offer important context for understanding regional particle dynamics. Compared to traditional methods such as sediment traps and bottle sampling, which often suffer from low spatial resolution and potential particle alteration during collection (Ramondenc et al., 2016), the UVP provides continuous, high-resolution *in situ* imaging of marine particles. It enables detailed quantification of particle abundance, size distribution, and volume concentration across the entire water column with minimal disturbance, offering new insights into particle-mediated carbon export processes in this area. When compared to UVP data from other oceanic regions, our findings fall within the broad range reported for oligotrophic to mesotrophic systems, while also highlighting the role of environmental variability in shaping particle distributions (Table 2). The particle abundance in the SCS continental slope (0–783 particles L^{-1}, mean ± SD: 68 ± 69 particles L^{-1}) is comparable to observations in regions like the HNLC (High Nutrient, Low Chlorophyll) stations of the Southern Ocean (0–500 particles L^{-1}; Jouandet et al., 2011) and higher than the Equatorial Pacific mesopelagic zone (1–4 particles L^{-1}; Pretty, 2019). However, it is notably lower than the particle abundance during an iron-fertilized bloom station in the Southern Ocean (1400 ± 200 particles L^{-1}; Jouandet et al., 2011), where artificial nutrient enrichment significantly boosted particle production. This discrepancy underscores the influence of localized biogeochemical conditions on particle abundance. In terms of particle volume concentration (PVC), the SCS continental slope exhibits values ranging from 0–6.7 mm^3 L^{-1} (mean ± SD: 0.3 ± 0.4 mm^3 L^{-1}), aligning well with the Gulf of Alaska shelf (0.1–1 mm^3 L^{-1}; Turner et al., 2017) and the HNLC stations in the Southern Ocean (0–50 mm^3 L^{-1}; Jouandet et al., 2011). Conversely, these values are lower compared to the iron-fertilized bloom stations (183 ± 34 mm^3 L^{-1}; Jouandet et al., 2011), reflecting the significant impact of primary production and aggregation processes. Overall, the particle abundance and volume concentration observed in this study are consistent with those from other oligotrophic and mesotrophic regions. The differences between regions highlight the importance of local environmental factors, including nutrient availability, primary production, and physical oceanographic conditions, in shaping marine particle dynamics.

https://doi.org/10.5194/egusphere-2025-2034
Preprint. Discussion started: 27 May 2025
© Author(s) 2025. CC BY 4.0 License.

438 **Table 2 Comparison of particle abundances and volume concentrations in this study with those in other studies. —:**
439 **no data.**

Location	Depth (m)	Particle abundance range (mean±SD) (# L^{-1})	PVC range (mean±SD) (mm^3 L^{-1})	Reference
The North Mediterranean	0-400	0-80	—	Gorsky et al., 2000
The Ligurian Sea	0-1000	0-1108	—	Stemmann et al., 2008
Off Cape Blanc, NW Africa	0-80	30-100	—	Iversen et al., 2010
The HNLC stations in the Southern Ocean	0-100	0-500	0-50	Jouandet et al., 2011
Iron-fertilized bloom station in the Southern Ocean	0-100	1400 ± 200	183 ± 34	Jouandet et al., 2011
Southeast of Kerguelen Island (Southern Ocean)	0-100	90 ± 5	0.3 ± 0.1	Jouandet et al., 2014
The Gulf of Alaska shelf	0-40	—	0.1-1	Turner et al., 2017
The Equatorial Pacific	200-1000	1-4	—	Pretty 2019
The North Pacific Gyre	>1000	0.1-0.3	—	Pretty 2019
The eastern tropical North Pacific	160-500	1-10	—	Cram et al., 2022
Station ALOHA (22.75ºN, 158.00ºW)	0-75	50-125	—	James 2024
SCS continental slope	0-800	0-783 (68 ± 69)	0.0-6.7 (0.3 ± 0.4)	This study

440

https://doi.org/10.5194/egusphere-2025-2034
Preprint. Discussion started: 27 May 2025
© Author(s) 2025. CC BY 4.0 License.

4.2 Distribution characteristics and influencing factors of marine particles

Horizontally, particle abundance and PVC exhibited clear cross-shelf gradients, with higher values observed at the inner slope stations, and a decreasing trend toward offshore waters (Fig. 5a, d; Fig. 6a, d). This nearshore-to-offshore decline is consistent with previous findings. Forest et al. (2012) reported a tow-order-of-magnitude drop in large particle abundance from the shelf to the basin across the Mackenzie shelf (Arctic Ocean), while Turner et al. (2017) observed the highest particle concentrations near freshwater-influenced shelf breaks in the Gulf of Alaska, decreasing over mid-shelf regions. In the present study, the shallow nutricline observed at inner slope stations (Fig. 3a, d) enhances light availability in the SCM layer, likely promoting higher Chl *a* concentrations (Fig. 4a, b). The resulting increase in phytoplankton biomass may stimulate organic matter production and particle aggregation (Panaïotis et al., 2024), thereby contributing to elevated particle concentrations. Additionally, the proximity to the continental margin increases exposure to lithogenic inputs from terrestrial sources (Liu et al., 2016), further enhancing particle loads in slope waters. In contrast, Transect 3 exhibited elevated particle abundance and PVC in the upper water column at offshore stations S11 and S12 (Fig. 5g; Fig. 6g). Sea level anomaly (SLA) data revealed that these stations were positioned at the periphery of a cyclonic eddy (Fig. 1d). Given their offshore location (> 200 km from land), the particle enrichment at these sites is unlikely to stem from terrestrial inputs and instead reflects localized biological production. Mesoscale eddies are known to modulate particle dynamics through their effect on nutrient entrainment, biological productivity, and physical retention (Maiti et al., 2008). Cyclonic eddies, in particular, induce upward vertical transport that enhances nutrient supply to the euphotic zone, stimulating phytoplankton growth and aggregate formation (Kahru et al., 2007). Furthermore, convergence and retention zones along the eddy periphery can trap suspended and sinking particles, facilitating localized particle accumulation (Accardo et al., 2025). In our study, the elevated particle concentrations at S11 and S12 support this mechanism (Fig. 5), suggesting a coupling between eddy-driven nutrient enhancement and biological particle production. UVP imagery also revealed that large phytoplankton cells and zooplankton dominated the particle assemblages at these sites (Fig. 7), reinforcing the biological origin of the observed signal.

At mid-slope stations S2 and S10, anomalously high particle abundance was detected in the deep water column (Fig. 5a, g). However, these elevated concentrations were primarily composed of small particles, resulting in no corresponding increase in PVC (Fig. 6a, g). This particle size structure suggests that the deep-layer signal reflects fine suspended material rather than rapidly sinking aggregates. One plausible explanation for this deep particle enrichment is the presence of intermediate nepheloid layers, which form due to resuspension and lateral transport of fine particles along the slope (Chen et al., 2024). These layers are often associated with bottom boundary layer dynamics or internal waves, which can enhance the lateral advection of resuspended material from the continental margin into the deep slope region (Jia et al., 2019).

Both particle abundance and PVC in the study area showed a decreasing trend with increasing depth. Waters shallower than 200 m exhibited significantly higher particle abundance and PVC compared to deeper waters (Supplementary Fig. S4). Although elevated particle abundance was observed in the deep layers at station S2 and S10, their corresponding PVC values remained relatively low (Fig. 5, 6), indicating a predominance of small-sized particles at these depths. The decrease in particle concentration from 0–200 m to 200–800 m water depth on the SCS continental slope highlights distinct vertical processes influencing particle dynamics in this region. The elevated particle concentrations in the upper 200 m can primarily be attributed to biological production in the euphotic zone, where photosynthetic activity by phytoplankton dominates (Fig. 4). This

https://doi.org/10.5194/egusphere-2025-2034
Preprint. Discussion started: 27 May 2025
© Author(s) 2025. CC BY 4.0 License.

process could generate abundant organic matter, including individual cells, aggregates, and detritus, which constitute a significant portion of the observed particles (Panaïotis et al., 2024). Additionally, processes such as grazing by zooplankton, production of fecal pellets, and aggregation further contribute to particle abundance in the upper water column (Fender et al., 2019). In contrast, the lower particle concentrations in the 200–800 m depth range reflect the combined effects of particle export, degradation, and remineralization during vertical transport. As particle sink, a substantial portion undergoes biological consumption by heterotrophic organisms or is remineralized into dissolved organic matter (Guidi et al., 2008b; Turner, 2015). Furthermore, smaller particles, which dominate in size below the euphotic zone, are more susceptible to disaggregation with slower sinking rates (Durkin et al., 2015). These observations align with global trends, where particle concentrations typically decrease with depth, driven by the attenuation of biological and physical processes (Kiko et al., 2022). The pronounced vertical particle concentration gradient underscores the efficiency of biological and microbial processes in the upper mesopelagic zone, which mediate the transfer and transformation of organic carbon.

4.3 Implications for carbon export and comparisons between large and small particles

The POC export flux estimated from the UVP-derived particle size distribution in the SCS continental slope ranged from 3.4 to 302.4 mg C m^{-2} d^{-1}, with an average of 33.6 mg C m^{-2} d^{-1} in this study. These values are broadly consistent with previous estimates using independent methodologies in the SCS. For instance, Cai et al. (2015) reported POC export fluxes at 100 m depth in the northern slope of the SCS based on $^{234}Th/^{238}U$ disequilibrium, ranging from 24.0 to 76.8 mg C m^{-2} d^{-1}. Similarly, Zhang et al. (2020) estimated POC export fluxes of 20.3 ± 2.2 mg C m^{-2} d^{-1} at 120 m depth in the core of an anticyclonic eddy in the SCS slope region. The agreement between these independent measurements suggests that UVP-based approaches provide a reasonable information of POC export fluxes in the SCS continental margin. Our results also align with UVP-based POC flux estimates in other oceanic regions. For example, Ramondenc et al. (2016) reported a wide range of POC export fluxes in the Mediterranean Sea, spanning 0 to 504 mg C m^{-2} d^{-1}, while Fender et al. (2019) documented an average flux of 42.1 mg C m^{-2} d^{-1} in the California Current Ecosystem. These comparisons highlight the applicability of UVP-based particle flux estimations across diverse oceanic settings.

The UVP data reveal a clear dominance of small particles (ESD<0.5 mm) in terms of abundance throughout the water column, accounting for over 97% of total particle abundance (Fig. 5). However, when examining volume concentration, a contrasting pattern emerges: small particles contribute a lower proportion to the total particle volume compared to large particles (ESD≥0.5 mm) (Fig. 6). Specifically, in the 0–200 m layer, large particles account for an average of 61% of the total volume, whereas small particles contribute only 39%. This trend shifts slightly in deeper waters (>200 m), where the contribution of large particles decreases to 52%, and small particles increase to 48% (Fig. 6). Although small particles overwhelmingly dominated particle abundance across the slope region of the SCS, their contribution to the POC flux was notably lower than that of large particles (Fig. 10). This apparent disconnect between numerical dominance and carbon export efficiency underscores the importance of particle size in determining vertical carbon flux. Smaller particles tend to have lower sinking velocities due to their higher surface-area-to-volume ratios and reduced mass, which makes them more susceptible to microbial degradation, grazing, and disaggregation in the upper ocean (Riley et al., 2012; Durkin et al., 2015). In contrast, large particles—such as fast-sinking marine snow aggregates, fecal pellets, and large phytoplankton or zooplankton carcasses—settle more rapidly and are therefore more efficient vehicles for

https://doi.org/10.5194/egusphere-2025-2034
Preprint. Discussion started: 27 May 2025
© Author(s) 2025. CC BY 4.0 License.

transporting organic carbon to depth (Iversen et al., 2010; Forest et al., 2012). Previous studies have also documented that, despite being numerically less abundant, large particles can disproportionately contribute to the bulk of vertical carbon flux. Steinberg et al. (2023) found that large aggregates and zooplankton fecal pellets were the primary drivers of POC flux in the northeast subarctic Pacific, due to their rapid sinking and high carbon content. Similarly, Dunne et al. (2007) highlighted that small particles are more likely to be retained and remineralized in the upper water column, limiting their export potential in the ocean. In our study, the dominance of small particles in abundance but their relatively minor role in POC flux suggests that carbon export efficiency in the SCS slope region is largely regulated by the production and fate of large, fast-sinking particles.

The vertical partitioning of POC flux between small particles and large particles also revealed distinct depth-dependent patterns (Supplementary Fig. S5). Specifically, the relative contribution of small particles to total POC flux increased progressively with depth (Fig. S3a), while that of large particles showed a corresponding decline (Fig. S3b). This trend suggests that, although large particles dominate carbon export in the upper ocean, their influence diminishes with depth, whereas small particles become increasingly important in the mesopelagic zone and below. Several mechanisms may account for this shift. Large particles, such as fecal pellets and marine snow aggregates, typically sink rapidly and can reach depth with relatively little degradation (Turner, 2015). However, they are also more prone to fragmentation and microbial decomposition during descent, especially in the upper mesopelagic zone (Stamieszkin et al., 2017). As these large particles disaggregate, they contribute to the pool of smaller, slower-sinking particles, thereby increasing the relative contribution of small particles to the total flux at greater depths. In contrast, small particles—although less efficient in transporting carbon due to their slower sinking velocities and higher residence times—can persist longer in the water column. Their accumulation with depth may reflect both the transformation of larger particles and the presence of suspended or laterally transported material from nepheloid layers (Zhou et al., 2020; Chen et al., 2024). These observations highlight the dynamic nature of particle flux attenuation and transformation with depth.

4.4 Influence of mesoscale eddies on particle distribution and carbon flux

Mesoscale eddies exert a significant influence on the distribution and export of particles in the ocean, primarily through their effects on vertical nutrient fluxes, biological production, and particle transport (Shih et al., 2020; Zhang et al., 2020). In this study, two contrasting eddy regimes were encountered: an anticyclonic eddy influencing stations S4 and S5, and a cyclonic eddy encompassing the periphery of stations S11 and S12 (Fig. 1d). The comparison between cyclonic and anticyclonic eddy stations revealed distinct differences in nutrient concentrations, phytoplankton biomass, particle characteristics and POC fluxes, highlighting the contrasting impacts of these two types of mesoscale eddies on carbon export processes. At the cyclonic eddy stations (S11 and S12), nutrient concentrations in the upper 50 m, particularly nitrate and phosphate, were significantly elevated compared to those at the anticyclonic eddy stations (S4 and S5) (Supplementary Fig. S2, *t*-test, $p < 0.01$). This nutrient enrichment likely resulted from upwelling processes induced by the cyclonic eddy, which supplied subsurface nutrients to the euphotic zone (Guidi et al., 2012; Zhou et al., 2021). Consequently, phytoplankton biomass, reflected by Chl *a* concentrations, was also higher in the cyclonic eddy region (Fig. S2d). Enhanced primary production stimulated by nutrient availability led to greater production of organic particles. In response to elevated phytoplankton biomass, particle abundance and PVC were substantially higher at the cyclonic eddy stations (Fig. S3, *t*-test, $p < 0.01$). This increase in particulate material contributed to the elevated

https://doi.org/10.5194/egusphere-2025-2034
Preprint. Discussion started: 27 May 2025
© Author(s) 2025. CC BY 4.0 License.

POC fluxes observed at S11 and S12 across all depths. Notably, POC fluxes at these stations exceeded 100 mg C m^{-2} d^{-1} in the upper layers and remained relatively high at deeper depths (Fig. 9), suggesting efficient vertical transport of organic carbon facilitated by particle aggregation and rapid sinking. In contrast, anticyclonic eddies are typically associated with downwelling and thermocline deepening, leading to nutrient limitation and reduced surface productivity (Stramma et al., 2013). This pattern is evident in the nutrient and Chl *a* distributions observed at stations S4 and S5 in this study (Supplementary Fig. S2). The low productivity in this region likely contributed to the reduced particle concentrations and diminished carbon fluxes (Supplementary Fig. S3). Overall, cyclonic eddies enhanced carbon export by promoting nutrient injection, stimulating primary production, and facilitating the formation and vertical transfer of sinking particles. In contrast, anticyclonic eddies suppressed these processes, leading to lower particle abundance and weaker POC fluxes. These findings emphasize the pivotal role of mesoscale physical dynamics in regulating biological pump efficiency and carbon sequestration in oligotrophic ocean regions.

In the SCS, previous studies have highlighted the critical role of mesoscale eddies in regulating biogeochemical processes. For example, Li et al. (2017) found that the POC flux in cyclonic eddies was 41% higher than that during the non-cyclonic eddy period in the central SCS. Liu et al. (2020) studied zooplankton community structure in the northern SCS and found that decreased zooplankton biomass, abundances, and biovolumes were observed in the anticyclonic eddy compared to the edge and outside of the anticyclonic eddy. Shih et al. (2020) investigated the effect of eddies (cold and warm eddies) on the nutrient supply to the euphotic zone and the organic carbon export in the northern SCS, and found that the POC flux associated with the cold eddies was significantly higher than that associated with the warm eddy. This study, based on high-resolution observations of particle distribution and associated POC fluxes, reveals the contrasting effects of cyclonic and anticyclonic eddies on particle production and carbon export. Cyclonic eddies in the SCS can act as biological pump enhancers, particularly along the slope regions where topography and eddy interactions are complex. In contrast, anticyclonic eddies, by suppressing the upward transport of nutrients, can lead to reduced biological production and consequently lower carbon export.

4.5 Data uncertainties

The high-resolution UVP observations allowed us to capture fine-scale vertical and spatial variability in particle abundance, PVC, and POC fluxes, which have been difficult to resolve using conventional sampling techniques. While this study provides valuable data and information, its limitations should also be acknowledged. The estimation of particle size and abundance was based on data from the UPV, which, despite its utility for *in situ* imaging, has limited sensitivity to particles smaller than ~100 μm and may underestimate the contribution of very fine particles to the total POC flux (Picheral et al., 2010). The conversion of particle volume to carbon flux relies on empirical relationships that may not fully capture spatial and temporal variability in particle composition and carbon content in the study area (Guidi et al., 2008a; Fender et al., 2019). Future studies incorporating direct flux measurements (e.g., sediment traps or thorium-based methods) would help reduce uncertainties and improve the quantification of particle-mediated carbon export.

5 Conclusion

Using high-resolution *in situ* observations from the UPV, this study provides a detailed characterization of

https://doi.org/10.5194/egusphere-2025-2034
Preprint. Discussion started: 27 May 2025
© Author(s) 2025. CC BY 4.0 License.

particle distributions and particle-mediated carbon fluxes along the continental slope of the SCS. The results demonstrate distinct spatial and vertical patterns in particle abundance and POC flux, shaped by hydrographic structure, biological production, and mesoscale physical processes. Small particles (ESD < 500 μm) overwhelmingly dominated in numerical abundance throughout the water column, but large particles (ESD ≥ μm) contributed disproportionately to vertical carbon export due to their higher sinking velocities. Mesoscale eddies were found to significantly modulate particle dynamics and export efficiency. Stations located at the edge of a cyclonic eddy exhibited elevated particle concentrations and POC fluxes, whereas those within an anticyclonic eddy displayed markedly reduced values. These contrasting signatures reflect the differential impacts of mesoscale physical processes on nutrient availability and particle production. The contribution of small particles to POC flux increased with depth, suggesting that disaggregation processes and lateral transport mechanisms, such as nepheloid layer formation, play a role in deep particle dynamics.

This study represents one of the first efforts to apply size-resolved UVP observations to characterize depth-dependent particle fluxes in the SCS. By resolving the relative roles of small and large particles and linking their export patterns to mesoscale forcing, our results provide new insights into the size-selective processes governing vertical carbon transport in marginal seas. These findings highlight the value of combining optical imaging tools with hydrographic context to constrain particle-mediated carbon export, which offers process-level evidence that can inform the representation of size-structured export fluxes in global biogeochemical models.

Data Availability Statement

Data available on request from the authors.

Author Contribution

SG: Conceptualization, Data curation, Formal analysis, Methodology, Software, Visualization, Writing-original draft preparation. MZ: Data curation, Formal analysis, Investigation, Methodology, Validation. WX: Data curation, Methodology. SZ: Investigation. SL: Data curation, Investigation. YW: Data curation, Investigation. JD: Data curation. CZ: Visualization. XS: Conceptualization, Data curation, Funding acquisition, Project administration, Supervision, Writing-review&editing.

Competing interests

The authors declare that they have no conflict of interest.

Disclaimer

Publisher's note: Copernicus Publications remains neutral with regard to jurisdictional claims made in the text, published maps, institutional affiliations, or any other geographical representation in this paper. While Copernicus Publications makes every effort to include appropriate place names, the final responsibility lies with the authors.

Acknowledgements

We thank the crew and captain of the R/V *Nanfeng* for the logistic support during the cruise. This work was supported by the National Key Research and Development Program of China (No. 2024YFE0114300), the

https://doi.org/10.5194/egusphere-2025-2034
Preprint. Discussion started: 27 May 2025
© Author(s) 2025. CC BY 4.0 License.

National Natural Science Foundation of China (No. 32371619, U2006206), the National Basic Research Program of China (No. 2014CB441504), the International Partnership Program of Chinese Academy of Sciences (No. 133137KYSB20200002, 121311KYSB20190029).

Financial support

This research has been supported by the National Key Research and Development Program of China (No. 2024YFE0114300), the National Natural Science Foundation of China (No. 32371619, U2006206), the National Basic Research Program of China (No. 2014CB441504), the International Partnership Program of Chinese Academy of Sciences (No. 133137KYSB20200002, 121311KYSB20190029).

References

Accardo, A., Laxenaire, R., Baudena A., Speich, S., Kiko, R., Stemman, L.: Intense and localized export of selected marine snow types at eddy edges in the South Atlantic Ocean, Biogeosciences, 22, 1183–1201, https://doi.org/10.5194/bg-22-1183-2025, 2025.

Boss, E., Guidi, L., Richardson, M. J., Stemmann, L., Gardner, W., Bishop, J. K., Anderson, R. F., Sherrell, R. M.: Optical techniques for remote and in-situ characterization of particles pertinent to GEOTRACES. Prog. Oceanogr., 133, 43–54, https://doi.org/10.1016/j.pocean.2014.09.007, 2015.

Boyd, P. W., Claustre, H., Levy, M., Siegel, D. A., Weber, T.: Multi-faceted particle pumps driven carbon sequestration in the ocean. Nature, 568(7752), 327–335, https://doi.org/10.1038/s41586-019-1098-2, 2019.

Cai, P., Zhao, D., Wang, L., Huang, B., Dai, M.: Role of particle stock and phytoplankton community structure in regulating particulate organic carbon export in a large marginal sea. J. Geophys. Res., 120, 2063–2095, https://doi.org/10.1002/2014JC010432, 2015.

Chen, T., Liu, X. L., Bian, C. W., Zhang, S. T., Ji, C. S., Wu, Z. S., Jia, Y. G.: Nepheloid layer structure and variability along the highly energetic continental margin of the northern South China Sea. J. Geophys. Res., 129(2), e2023JC020072, https://doi.org/10.1029/2023JC020072, 2024.

Clements, D. J., Yang, S., Weber, T., McDonnell, A. M. P., Kiko, R., Stemmann, L., Bianchi, D.: New estimate of organic carbon export from optical measurements reveals the role of particle size distribution and export horizon. Global Biogeochem. Cy., 37, e2022GB007633, https://doi.org/10.1029/2022GB007633, 2023.

Cram, J. A., Weber, T., Leung, S. W., McDonnell, A. M., Liang, J. H., Deutsch, C.: The role of particle size, ballast, temperature, and oxygen in the sinking flux to the deep sea. Global Biogeochem. Cy., 32(5), 858–876, https://doi.org/10.1029/2017GB005710, 2018.

Cram, J. A., Fuchsman, C. A., Duffy, M. E., Pretty, J. L., Lekanoff, R. M., Neibauer, J. A., Leung, S. W., Huebert, K. B., Weber, T. S., Bianchi, D., Evans, N., Devol, A. H., Keil, R. G., McDonnell, A. M. P.: Slow particle remineralization, rather than suppressed disaggregation, drives efficient flux transfer through the eastern tropical North Pacific oxygen deficient zone. Global Biogeochem. Cy., 36, e2021GB007080, https://doi.org/10.1029/2021GB007080, 2022.

Dai, S., Zhao, Y. F., Liu, H. J., Hu, Z. Y., Zheng, S., Zhu, M. L., Guo, S. J., Sun, X. X.: The effects of a warm-core eddy on chlorophyll *a* distribution and phytoplankton community structure in the northern South China Sea in spring 2017. J. Marine Syst., 210, 103396, https://doi.org/10.1016/j.jmarsys.2020.103396, 2020.

https://doi.org/10.5194/egusphere-2025-2034
Preprint. Discussion started: 27 May 2025
© Author(s) 2025. CC BY 4.0 License.

Dunne, J. P., Sarmiento, J. L., Gnanadesikan, A: A synthesis of global particle export from the surface ocean and cycling through the ocean interior and on the seafloor. Global Biogeochem. Cy., 21(4), GB4006, https://doi.org/10.1029/2006GB002907, 2007.

Durkin, C. A., Estapa, M. L., Buesseler, K. O.: Observations of carbon export by small sinking particles in the upper mesopelagic. Mar. Chem., 175, 72–81, https://doi.org/10.1016/j.marchem.2015.02.011, 2015.

Fender, C. K., Kelly, T. B., Guidi, L., Ohman, M. D., Smith M, C., Stukel, M. R.: Investigating particle size-flux relationships and the biological pump across a range of plankton ecosystem states from coastal to oligotrophic. Front. Mar. Sci., 6, 603, https://doi.org/10.3389/fmars.2019.00603, 2019.

Forest, A., Stemmann, L., Picheral, M., Burdorf, L., Robert, D., Fortier, L., Babin, M.: Size distribution of particles and zooplankton across the shelf-basin system in southeast Beaufort Sea: combined results from an Underwater Vision Profiler and vertical net tows. Biogeosciences, 9, 1301–1320, https://doi.org/10.5194/bg-9-1301-2012, 2012.

Gorsky, G., Picheral, M., Stemmann, L.: Use of the Underwater Video Profiler for the study of aggregate dynamics in the North Mediterranean. Estuar. Coast. Shelf S., 50, 121–128, https://doi.org/10.1006/ecss.1999.0539, 2000.

Guidi, L., Stemmann, L., Legendre, L., Picheral, M., Prieur, L., Gorsky, G: Vertical distribution of aggregates (>100 µm) and mesoscale activity in the Northeastern Atlantic: effects on the deep vertical export of surface carbon. Limnol. Oceanogr., 52, 7–18, https://doi.org/10.4319/lo.2007.52.1.0007, 2007.

Guidi, L., Jackson, G. A., Stemmann, L., Miquel, J. C., Picheral, M., Gorsky, G: Relationship between particle size distribution and flux in the mesopelagic zone. Deep-Sea Res. PT I, 55, 1364–1374, https://doi.org/10.1016/j.dsr.2008.05.014, 2008a.

Guidi, L., Gorsky, G., Claustre, H., Miquel, J. C., Picheral, M., Stemmann, L.: Distribution and fluxes of aggregates >100 µm in the upper kilometer of the South-Eastern Pacific. Biogeosciences, 5, 1361–1372, https://doi.org/10.5194/bg-5-1361-2008, 2008b.

Guidi, L., Stemmann, L., Jackson, G. A., Ibanez, F., Claustre, H., Legendre, L., Picheral, M., Gorsky, G.: Effects of phytoplankton community on production, size, and export of large aggregates: a world-ocean analysis. Limnol. Oceanogr., 54(6), 1951–1963, https://doi.org/10.4319/lo.2009.54.6.1951, 2009.

Guidi, L., Calil, P. H. R., Duhamel, S., Björkman, K. M., Doney, S. C., Jackson, G. A., Li, B. L., Church, M. J., Tozzi, S., Kolber, Z. S., Richards, K. J., Fong, A. A., Letelier, R. M., Gorsky, G., Stemmann, L., Karl, D. M.: Does eddy-eddy interaction control surface phytoplankton distribution and carbon export in the North Pacific Subtropical Gyre? J. Geophys. Res., 117, G02024, https://doi.org/10.1029/2012JG001984, 2012.

Guidi, L., Legendre, L., Reygondeau, G., Uitz, J., Stemmann, L., Henson, S. A.: A new look at ocean carbon remineralization for estimating deepwater sequestration. Global Biogeochem. Cy., 29(7), 1044–1059, https://doi.org/10.1002/2014GB005063, 2015.

Guidi, L., Chaffron, S., Bittner, L., Eveillard, D., Larhlimi, A., Roux, S., Darzi, Y., Audic, S., Berline, L., Brum, J. R., Coelho, L. P., Espinoza, J. C. I., Malviya, S., Sunagawa, S., Dimier, C., Kandels-Lewis, S., Picheral, M., Poulain, J., Searson, S., Consortium Coordinators, T . O., Stemmann, L., Not, F., Hingamp, P., Speich, S., Follows, M., Karp-Boss, L., Boss, E., Ogata, H., Pesant, S., Weissenbach, J., Wincker, P, Acinas, S. G., Bork, P., de Vargas, C., Iudicone, D., Sullivan, M. B., Raes, J., Karsenti, E., Bowler, C., Gorsky, G.: Plankton networks driving carbon export in the oligotrophic ocean. Nature, 532, 465–470, https://doi.org/10.1038/nature16942,

https://doi.org/10.5194/egusphere-2025-2034
Preprint. Discussion started: 27 May 2025
© Author(s) 2025. CC BY 4.0 License.

2016.

Hong, Q. Q., Peng, S. Y., Zhao, D. C., Cai, P. H.: Cross-shelf export of particulate organic carbon in the northern South China Sea: Insights from a ^{234}Th mass balance. Prog. Oceanogr., 193, 102532, https://doi.org/10.1016/j.pocean.2021.102532, 2021.

Iversen, M. H., Nowald, N., Ploug, H., Jackson, G. A., Fischer, G.: High resolution profiles of vertical particulate organic matter export off Cape Blanc, Mauritania: degradation processes and ballasting effects. Deep-Sea Res. PT I, 57(6), 771–784, https://doi.org/10.1016/j.dsr.2010.03.007, 2010.

James, R.: Applications of the Underwater Vision Profiler for particle annotation in the oligotrophic North Pacific subtropical gyre, M.S. thesis, University of Hawai at Manoa, USA, 63 pp., 2024.

Jia, Y. G., Tian, Z. C., Shi, X. F., Liu, J. P., Chen, J. X., Liu, X. L., Ye, R. J., Ren, Z. Y., Tian, J. W.: Deep-sea sediment resuspension by internal solitary waves in the northern South China Sea. Sci. Rep., 9, 12137, https://doi.org/10.1038/s41598-019-47886-y, 2019.

Jouandet, M. P., Trull, T. W., Guidi, L., Picheral, M., Ebersbach, F., Stemmann, L., Blain, S.: Optical imaging of mesopelagic particles indicates deep carbon flux beneath a natural iron-fertilized bloom in the Southern Ocean. Limnol. Oceanogr., 56(3), 1130–1140, https://doi.org/10.4319/lo.2011.56.3.1130, 2011.

Jouandet, M. P., Jackson, G. A., Carlotti, F., Picheral, M., Stemmann, L., Blain, S.: Rapid formation of large aggregates during the spring bloom of Kerguelen Island: observations and model comparisons. Biogeosciences, 11, 4393–4406, https://doi.org/10.5194/bg-11-4393-2014, 2014, 2014.

Kahru, M., Mitchell, B. G., Gille, S. T., Hewes, C. D., Holm-Hansen, O.: Eddies enhance biological production in the Weddell-Scotia Confluence of the Southern Ocean. Geophys. Res. Lett., 34, L14603, https://doi.org/10.1029/2007GL030430, 2007.

Kiko, R., Biastoch, A., Brandt, P., Cravatte, S., Hauss, H., Hummels, R., Kriest, I., Marin, F., MaDonnell, A. M. P., Oschlies, A., Picheral, M., Schwarzkopf, F. U., Thurnherr, A. M., Stemmann, L.: Biological and physical influences on marine snowfall at the equator. Nat. Geosci., 10(11), 852–858, https://doi.org/10.1038/ngeo3042, 2017.

Kiko, R., Picheral, M., Antoine, D., Babin, M., Berline, L., Biard, T., Boss, E., Brandt, P., Carlotti, F., Christiansen, S., Coppola, L., de la Cruz, L., Diamond-Riquier, E., de Madron, X. D., Elineau, A., Gorsky, G., Guidi, L., Hauss, H., Irisson, J. O., Karp-Boss, L., Karstensen, J., Kim, D., Lekanoff, R. M., Lombard, F., Lopes, R. M., Marec, C., Mcdonnell, A. M. P., Niemeyer, D., Noyon, M., O'Daly, S. H., Ohman, M. D., Pretty, J. L., Rogge, A., Searson, S., Shibata, M., Tanaka, Y., Tanhua, T., Taucher, J., Trudnowska, E., Turner, J. S., Waite, A., Stemmann, L.: A global marine particle size distribution dataset obtained with the Underwater Vision Profiler 5. Earth Syst. Sci. Data, 14, 4315–4337, https://doi.org/10.5194/essd-14-4315-2022, 2022.

Kriest, I.: Different parameterizations of marine snow in a 1D-model and their influence on representation of marine snow, nitrogen budget and sedimentation. Deep-Sea Res. PT I, 49(12), 2133–2162, https://doi.org/10.1016/S0967-0637(02)00127-9, 2002.

Kwon, E. Y., Primeau, F., Sarmiento, J. L.: The impact of remineralization depth on the air-sea carbon balance. Nat. Geosci., 2(9), 630–635, https://doi.org/10.1038/ngeo612, 2009.

Li, H. L., Wiesner, M. G., Chen, J. F., Ling, Z., Zhang, J. J., Ran, L. H.: Long-term variation of mesopelagic biogenic flux in the central South China Sea: Impact of monsoonal seasonality and mesoscale eddy. Deep-Sea Res. PT I, 126, 62–72, https://doi.org/10.1016/j.dsr.2017.05.012, 2017.

Liu, H. J., Zhu, M. L., Guo, S. J., Zhao, X. H., Sun, X. X.: Effects of an anticyclonic eddy on the distribution and

https://doi.org/10.5194/egusphere-2025-2034
Preprint. Discussion started: 27 May 2025
© Author(s) 2025. CC BY 4.0 License.

community structure of zooplankton in the South China Sea northern slope. J. Marine Syst., 205, 103311, https://doi.org/10.1016/j.jmarsys.2020.103311, 2020.

Liu, J. A., Du, J. Z., Wu, Y., Liu, S. M.: Radium-derived water mixing and associated nutrient in the northern South China Sea. Front. Mar. Sci., 9, 874547, https://doi.org/10.3389/fmars.2022.874547, 2022.

Liu, Z. F., Zhao, Y. L., Colin, C., Stattegger, K., Wiesner, M. G., Huh, C. A., Zhang, Y. W., Li, X. J., Sompongchaiyakul, P., You, C. F., Huang, C. Y., Liu, J. T., Siringan, F. P., Le, K. P., Sathiamurthy, E., Hantoro, W. S., Liu, J. G., Tuo, S. T., Zhao, S. H., Zhou, S. W., He, Z. D., Wang, Y. C., Bunsomboonsakul, S., Li, Y.: Source-to-sink transport processes of fluvial sediments in the South China Sea. Earth-Sci. Rev., 153, 238–273, https://doi.org/10.1016/j.earscirev.2015.08.005, 2016.

Ma, Y. F., Zhou, K. B., Chen, W. F., Chen, J. H., Yang, J. T., Dai, M. H.: Partitioning of carbon export in the euphotic zone of the oligotrophic South China Sea. Biogeosciences, 20, 2013–2030, https://doi.org/10.5194/bg-20-2013-2023, 2023.

Maiti, K., Benitez-Nelson, C. R., Rii, Y., Bidigare, R.: The influence of a mature cyclonic eddy on particle export in the lee of Hawaii. Deep-Sea Res. PT II, 55(10-13), 1445–1460, https://doi.org/10.1016/j.dsr2.2008.02.008, 2008.

Panaïotis, T., Poteau, A., Riquier, É. D., Catalano, C., Courchet, L., Motreuil, S., Coppola, L., Picheral, M., Irisson, J. O.: Temporal evolution of plankton and particles distribution across a mesoscale front during the spring bloom. Limnol. Oceanogr., 9999, 1–15, https://doi.org/10.1002/lno.12566, 2024.

Picheral, M., Guidi, L., Stemmann, L., Karl, D. M., Iddaoud, G., Gorsky, G.: The Underwater Vision Profiler 5: an advanced instrument for high spatial resolution studies of particle size spectra and zooplankton. Limnol. Oceanogr-Meth., 8, 462–473, https://doi.org/10.4319/lom.2010.8.462, 2010.

Picheral, M., Catalano, C., Brousseau, D., Claustre, H., Coppola, L., Leymarie, E., Coindat, J., Dias, F., Fevre, S., Guidi, L., Irisson, J. O., Legendre, L., Lombard, F., Mortier, L., Penkerch, C., Rogge, A., Schmechtig, C., Thibault, S., Tixier, T., Waite, A., Stemmann, L.: The Underwater Vision Profiler 6: an imaging sensor of particle size spectra and plankton, for autonomous and cabled platforms. Limnol. Oceanogr-Meth., 20(2), 115–129, https://doi.org/10.1002/lom3.10475, 2022.

Pretty, J. L.: Particles in the Pacific: how productivity and zooplankton relate to particles in the deep sea. M.S., thesis, University of Alaska Fairbanks, USA, 41 pp., 2019.

Ramondenc, S., Madeleine, G., Lombard, F., Santinelli, C., Stemmann, L., Gorsky, G., Guidi, L.: An initial carbon export assessment in the Mediterranean Sea based on drifting sediment traps and the underwater vision profiler data sets. Deep-Sea Res. PT I, 117, 107–119, https://doi.org/10.1016/j.dsr.2016.08.015, 2016.

Riley, J. S., Sanders, R., Marsay, C., Le Moigne, F. A. C., Achterberg, E. P., Poulton, A. J.: The relative contribution of fast and slow sinking particles to ocean carbon export. Global Biogeochem. Cy., 26(1), https://doi.org/10.1029/2011GB004085, 2012.

Shih, Y. Y., Hung, C. C., Tuo, S. H., Shao, H. J., Chow, C. H., Muller, F. L. L., Cai, Y. H.: The impact of eddies on nutrient supply, diatom biomass and carbon export in the northern South China Sea. Front. Earth Sc-Switz, 8, 537332, https://doi.org/10.3389/feart.2020.537332, 2020.

Siegel, D. A., DeVries, T., Cetinić, I., Bisson, K. M.: Quantifying the ocean's biological pump and its carbon cycle impacts on global scales. Annu. Rev. Mar. Sci., 15(1), 329–356, https://doi.org/10.1146/annurev-marine-040722-115226, 2022.

Stamieszkin, K., Poulton, N. J., Pershing, A. J.: Zooplankton grazing and egestion shifts particle size distribution

© Author(s) 2025. CC BY 4.0 License.

in natural communities. Mar. Ecol. Prog. Ser., 575, 43–56, https://doi.org/10.3354/meps12212, 2017.

Steinberg, D. K., Stamieszkin, K., Maas, A. E., Durkin, C. A., Passow, U., Estapa, M. L., Omand, M. M., McDonnell, A. M. P., Karp-Boss, L., Galbraith, M., Siegel, D. A.: The outsized role of salps in carbon export in the subarctic northeast Pacific Ocean. Global Biogeochem. Cy., 37, e2022GB007523, https://doi.org/10.1029/2022GB007523, 2023.

Stemmann, L., Eloire, D., Sciandra, A., Jackson, G. A., Guidi, L., Picheral, M., Gorsky, G.: Volume distribution for particles between 3.5 to 2000 µm in the upper 200 m region of the South Pacific Gyre. Biogeosciences, 5, 299–310, https://doi.org/10.5194/bg-5-299-2008, 2008.

Stramma, L., Bange, H. W., Czeschel, R., Lorenzo, A., Frank, M.: On the role of mesoscale eddies for the biological productivity and biogeochemistry in the eastern tropical Pacific Ocean off Peru. Biogeosciences, 10, 7293–7306, https://doi.org/10.5194/bg-10-7293-2013, 2013.

Turner, J. T.: Zooplankton fecal pellets, marine snow, phytodetritus and the ocean's biological pump. Prog. Oceanogr., 130, 205–248, https://doi.org/10.1016/j.pocean.2014.08.005, 2015.

Turner, J. S., Pretty, J. L., McDonnell, A. M. P.: Marine particles in the Gulf of Alaska shelf system: Spatial patterns and size distributions from in situ optics. Cont. Shelf Res., 145, 13–20, https://doi.org/10.1016/j.csr.2017.07.002, 2017.

Wang, X., Zhang, J., Zhao, X., Chen, Z., Ying, Y., Li, Z., Xu, D., Liu, Z., Zhou, M.: Vertical distribution and diel migration of mesopelagic fishes on the northern slope of the South China Sea. Deep-Sea Res. PT II, 167, 128–141, https://doi.org/10.1016/j.dsr2.2019.05.009, 2019.

Wang, X. Y., Li, H. L., Zhang, J. J., Chen, J. F., Xie, X. H., Xie, W., Yin, K. D., Zhang, D. S., Ruiz-Pino, D., Kao, S. J.: Seamounts generate efficient active transport loops to nourish the twilight ecosystem. Sci. Adv., 10(26), eadk6833, 10.1126/sciadv.adk68, 2024a.

Wang, Z. Y., Fang, C., Yang, C. H., Zhang, G. Y., Sun, D.: Latitudinal gradient and influencing factors of deep-sea particle export along the Kyushu-Palau Ridge in the Philippine Sea. Sci. Total Environ., 906, 167460, https://doi.org/10.1016/j.scitotenv.2023.167460, 2024b.

Welschmeyer, N. A.: Fluorometric analysis of chlorophyll a in the presence of chlorophyll b and pheopigments. Limnol. Oceanogr., 39(8), 1985–1992, https://doi.org/10.4319/lo.1994.39.8.1985, 1994.

Xiu, P., Chai, F., Shi, L., Xue, H., Chao, Y.: A census of eddy activities in the South China Sea during 1993–2007. J. Geophys. Res., 115, C03012, https://doi.org/10.1029/2009JC005657, 2010.

Zhang, M., Wu, Y., Wang, F. Q., Xu, D. F., Liu, S. M., Zhou, M.: Hotspot of organic carbon export driven by mesoscale eddies in the slope region of the northern South China Sea. Front. Mar. Sci., 7, 444, https://doi.org/10.3389/fmars.2020.00444, 2020.

Zhang, W. J., Zhang, C., Zheng, S., Chen, Y. Y., Zhu, M. L., Sun, X. X.: Distribution of picophytoplankton in the northern slope of the South China Sea under environmental variation induced by a warm eddy. Mar. Pollut. Bull., 194, 115429, https://doi.org/10.1016/j.marpolbul.2023.115429, 2023.

Zhou, K. B., Dai, M. H., Maiti, K., Chen, W. F., Chen, J. H., Hong, Q. Q., Ma, Y. F., Xiu, P., Wang, L., Xie, Y. Y.: Impact of physical and biogeochemical forcing on particle export in the South China Sea. Prog. Oceanogr., 187, 102403, https://doi.org/10.1016/j.pocean.2020.102403, 2020.

Zhou, K. B., Benitez-Nelson, C. R., Huang, J., Xiu, P., Sun, Z. Y., Dai, M. H.: Cyclonic eddies modulate temporal and spatial decoupling of particulate carbon, nitrogen, and biogenic silica export in the North Pacific

https://doi.org/10.5194/egusphere-2025-2034
Preprint. Discussion started: 27 May 2025
© Author(s) 2025. CC BY 4.0 License.

Subtropical Gyre. Limnol. Oceanogr., 66(9), 3508–3522, https://doi.org/10.1002/lno.11895, 2021.